Quantum Information Using Nitrogen-Vacancy Centers In Diamond

Supervisor: Georg Braunbeck
Email: georg.braunbeck@wsi.tum.de
Walter Schottky Institut
Technische Universität München
Am Coulombwall 4
85748 Garching

March 20, 2018

Contents

1 Safety Instructions **2**

2 Introduction **2**

3 Theoretical Background **2**
3.1 Electron Paramagnetic Resonance . . . 2
3.2 Rotating Reference Frame . . . 2
3.2.1 Basics . . . 3
3.2.2 Visualization . . . 3
3.2.3 Time Evolution . . . 4
3.3 Pulse Sequences . . . 4
3.3.1 Rabi Sequence . . . 5
3.3.2 Ramsey Sequence . . . 5
3.3.3 Hahn Echo Sequence . . . 7
3.4 The Nitrogen-Vacancy Center . . . 7

4 Experimental Setup **9**

5 Experimental Protocol **10**
5.1 Preparation . . . 10
5.1.1 Laser . . . 10
5.1.2 Camera . . . 10
5.1.3 Microwave . . . 10
5.2 Measurement Tasks . . . 11

6 Additional Questions **11**

1 Safety Instructions

Please read the enclosed safety instructions carefully. Working on the experiment is not permitted until all participants confirm with their signatures that they have carefully read and fully understood the safety instructions.

2 Introduction

Quantum Computing might solve some computational problems, that could break current cryptography standards in the blink of an eye. Quantum Sensing applications might provide chemically resolved, three dimensional images of single molecules. Both fields depend on the possibility to read quantum information stored in quantum bits (qubits). Man systems, however, require ultra high vacuum, complex laser setups or cryogenic temperatures.

Fortunately, the recently rediscovered nitrogen-vacancy center in diamond allows readout in air atmosphere at room temperature enabled by a setup that is small enough to be easily carried by a single person. This lab course will take advantage of this and let the students perform qubit initialization, simple readout as well as pulsed measurement protocols to read out more advanced information than pure qubit state.

3 Theoretical Background

This section provides the theoretical background to conduct and understand the measurements of this advanced lab course. First, the concept of electron paramagnetic resonance (EPR) is explained, which lays the foundation to understand all following measurements. Then, the rotating frame is introduced to gain a more intuitive understanding of the following most common pulsed measurement protocols in the field of EPR. Finally, the nitrogen-vacancy center in diamond is presented, which will be our atomic-scale EPR system throughout this lab course.

3.1 Electron Paramagnetic Resonance

Electron paramagnetic resonance is the switching of an electron spin state, once it is "tuned into resonance" with an external excitation field. The details can be derived from the following spin Hamiltonian of an electron in an external magnetic field $\boldsymbol{B_0} = B_0 \cdot \hat{z}$:

$$\hat{\mathcal{H}} = g_e \mu_B \hat{S}_z B_0 \tag{1}$$

Here, g_e is the *Landé g*-factor of the electron, μ_B is the *Bohr magneton* and $\hat{S}_z$ is the z component of the electronic spin operator with spin quantum number $S = \frac{1}{2}$. This equation describes the linear energy increase / decrease with respect to the external field, depending on the electron's spin eigenvalue $m_\mathrm{S} = \pm\frac{1}{2}$. Such a B-field induced energy splitting is usually referred to as *Zeeman splitting* (Figure 1).

If the photon energy $\hbar\omega_{ph}$ of a driving field

$$\boldsymbol{B_1} = B_1(\hat{x} \cdot \sin(\omega_{ph} t + \hat{y} \cdot \cos(\omega_{ph} t))) \tag{2}$$

matches the energy splitting at a field B_0, the photons can be absorbed or cause a stimulated decay to switch the spin state. This is the so called resonance condition of EPR:

$$\hbar\omega_{ph} = g_e \mu_B B_0 \tag{3}$$

3.2 Rotating Reference Frame

While the basic effect of EPR can be understood in this simple picture, the effect of pulse length, pulse power and detuning of the driving field $\boldsymbol{B_1}$ requires a more sophisticated picture: the rotating reference frame. A detailed derivation of the rotating reference frame can be found in the book *Handbook of MRI pulse sequences* by M. A. Bernstein, K.F. King and X. J. Zhou in Chapter 1.2.

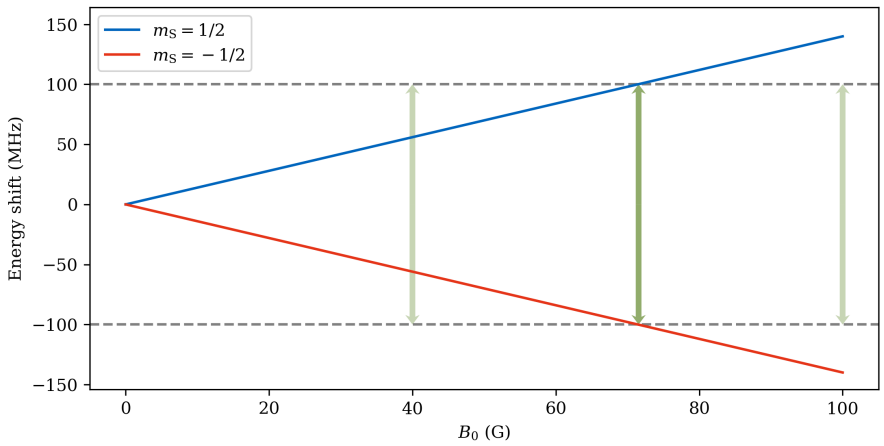

Figure 1: Zeeman splitting of a free electron spin in an external field B_0. The energy splitting of the two possible states $m_S = \pm\frac{1}{2}$ (blue and red line) is proportional to B_0. If the energy of a driving field (dashed gray lines) matches the splitting (rich green arrow), it induces transitions between the two states. In case of too high or too low energy (pale green arrows), transitions can not be driven.

3.2.1 Basics

The main idea is to simplify the representation of both the spin state and the excitation radiation. Similar to a classical magnetic moment, the spin is precessing with the *Larmor frequency* ω_L, defined by

$$\hbar\omega_L = g_e \mu_B B_0 \tag{4}$$

around $\boldsymbol{B_0}$, i.e. the z-axis. The magnetic component of a circularly polarized excitation beam propagating along the z-axis is also precessing around the z-axis, but with frequency ω_{ph} (Equation 2). By combining equations 3 and 4, that resonance can be rewritten as

$$\omega_L = \omega_{ph} \tag{5}$$

which further means, that in the case of resonance the excitation field and the spin precess at the same absolute frequency or with no relative frequency at all.

Thus, switching into a rotating reference frame precessing as well with frequency ω_{ph} around the z-axis, the excitation field becomes a constant vector in any case. The spin then precesses with the detuning frequency

$$\Delta\omega = \omega_{ph} - \omega_L \tag{6}$$

which usually is much lower than ω_L and in resonance it equals 0, rendering the spin static as well.

3.2.2 Visualization

In a rotating frame, the exact orientation of the constant vector $\boldsymbol{B_{1,\mathrm{rot}}}$ depends on its phase φ and detuning $\Delta\omega$:

$$\boldsymbol{B_{1,\mathrm{rot}}} = \cos(\varphi)B_1 \cdot \hat{x} + \sin(\varphi)B_1 \cdot \hat{y} + \frac{\Delta\omega}{\gamma} \cdot \hat{z} \tag{7}$$

Here, $\gamma = g_e\mu_B/\hbar$ is the gyromagnetic ratio. The phase φ defines the polar angle, while the detuning $\Delta\omega$ defines the azimuthal angle.

A spin state

$$|\psi\rangle = \cos\left(\frac{\theta}{2}\right)|\uparrow\rangle + \sin\left(\frac{\theta}{2}\right)e^{i\phi}|\downarrow\rangle\,, \tag{8}$$

where $|\uparrow\rangle$ and $|\downarrow\rangle$ are eigenstates, can simultaneously be visualized in the same reference frame. Formally, the coordinates x, y, z are calculated by

$$\begin{pmatrix} x \\ y \\ z \end{pmatrix} = \begin{pmatrix} \langle\psi| \sigma_x |\psi\rangle \\ \langle\psi| \sigma_y |\psi\rangle \\ \langle\psi| \sigma_z |\psi\rangle \end{pmatrix}, \tag{9}$$

with σ_i being the corresponding *Pauli matrix*.

Luckily, it can be shown, that the results follow simple rules: The z-component of the reference frame describes the excitation of the state. This results in θ being represented as the azimuthal angle:

$\|\psi\rangle$	θ	z
$\|\uparrow\rangle$	0	1
$\frac{\|\downarrow\rangle+\|\uparrow\rangle}{\sqrt{2}}$	$\frac{\pi}{2}$	0
$\|\downarrow\rangle$	π	-1

The quantum mechanical phase ϕ can further be expressed as the polar angle of the frame and is generated by a detuning between the quantum system and the excitation field, just as described for a classical picture by equation 6.

In summary, the spin state $|\psi\rangle$ introduced in equation 8 is represented by the so called *Bloch vector*

$$\vec{\psi} = \begin{pmatrix} \sin(\theta)\cos(\phi) \\ \sin(\theta)\sin(\phi) \\ \cos(\theta) \end{pmatrix}. \tag{10}$$

A comparison with common spherical coordinates already implies, that this state is always located on a sphere surface with radius $r = 1$, called the *Bloch sphere*.

3.2.3 Time Evolution

In general, the time evolution in the rotating frame of Bloch vector $\vec{\psi}$, induced by a driving field $\boldsymbol{B_{1,\mathrm{rot}}}$, is described by

$$\frac{d\vec{\psi}}{dt} = \gamma \cdot \vec{\psi} \times \boldsymbol{B_{1,\mathrm{rot}}}, \tag{11}$$

which becomes even more transparent for a specific case, that will be most prominent throughout this lab course: exciting $|\psi\rangle$ from the ground state applying a resonant $\boldsymbol{B_{1,\mathrm{rot}}}$ with phase $\varphi = 0$, rendering $\boldsymbol{B_{1,\mathrm{rot}}}$ a constant vector along the x-axis. For the first infinitely short time step, we get

$$\left(\frac{d\vec{\psi}}{dt}\right)_{\mathrm{t=0}} = \gamma \begin{pmatrix} 0 \\ 0 \\ 1 \end{pmatrix} \times \begin{pmatrix} B_1 \\ 0 \\ 0 \end{pmatrix} = \begin{pmatrix} 0 \\ \gamma B_1 \\ 0 \end{pmatrix}, \tag{12}$$

which for the following time steps results in a uniform rotation of our Bloch vector in the y-z-plane around the x-axis (Figure 2). The rotation speed is given by the field amplitude B_1. A pulse whose length has been adjusted to rotate the state vector by an angle of $\pi/2$ is called a $\pi/2$-pulse, accordingly for a π-pulse.

3.3 Pulse Sequences

With our knowledge from the previous section, we can now briefly discuss the effect of the basic pulse sequences used in EPR experiments. We will assume, that the state has been prepared in the ground state $|\uparrow\rangle$ at the beginning of the sequence. Further, $\boldsymbol{B_1}$ is assumed to be in resonance and the phase φ is chosen to be 0. As a result, the state vector's evolution is described by equation 12 during a pulse.

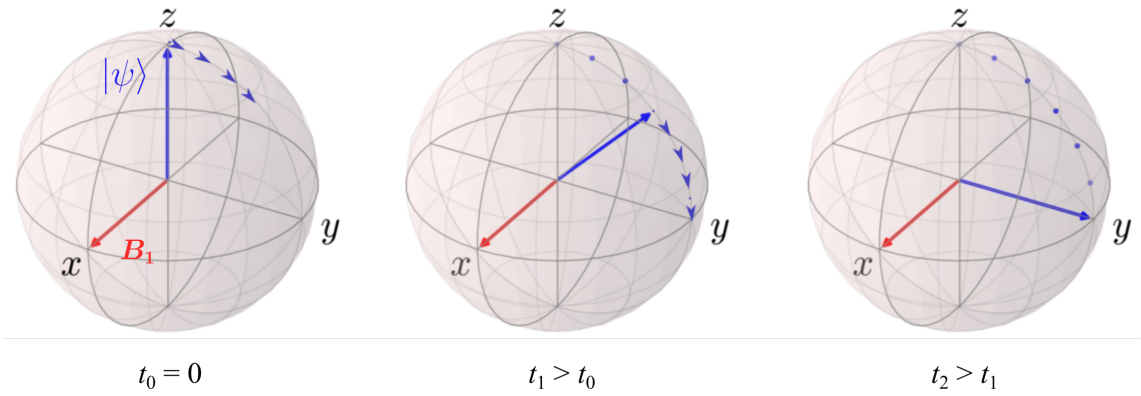

Figure 2: Time evolution of a resonantly driven spin visualized in the rotating frame. At $t_0 = 0$ the spin is in its ground state. According to equation 12, the state vector starts rotating along the y-z-plane towards the y-axis until it reaches the y-axis at $t = t_2$. However, the state vector will continue precessing in the same manner around $\boldsymbol{B_1}$ as long as the driving field is applied.

3.3.1 Rabi Sequence

As described by equation 12, the spin state vector $|\psi\rangle$ is constantly rotating around the x-axis with a rotation frequency purely defined by the excitation strength B_1. The resulting rotation angle is exclusively defined by the pulse length.

We can use this to probe the unknown but constant excitation strength B_1 by applying a *Rabi sequence*, named after the US American physicist *Isidor Isaac Rabi*, as shown in Figure 3 top. The spin is first initialized into its ground state, then rotated by a pulse of length T_p and finally its z-component is read out. During every subsequent iteration of the sequence, the pulse length is increased by ΔT_p, resulting in an increased rotation angle. This correlates the pulse length with the excitation level of the spin state. As the state vector keeps rotating along the spherical surface after arriving at the excited state, down to the ground state and then up again, the resulting graph of this measurement is a sine curve (Figure 3 bottom). The oscillation frequency depends on the resulting rotation angle after a given pulse length T_p and therefore on the excitation strength B_1.

A pulse is usually named after its rotation angle, as for example a spin flipping pulse is called a π-pulse with corresponding length T_π (Figure 3 bottom). The oscillation frequency, also called *Rabi frequency* Ω, is then defined as:

$$\Omega = \frac{2\pi}{T_{2\pi}}. \tag{13}$$

3.3.2 Ramsey Sequence

In resonance, a spin is rotating with the same frequency as the rotating frame itself and thus frozen within the reference frame in absence of any pulse. A resonant π-pulse as determined by a Rabi sequence measurement would therefore invert the spin excitation even if it is sliced up into an arbitrary number of sub-pulses, as long as the sum over all sub-pulse lengths is T_π. In the case $\Delta\omega \neq 0$ however, as described in section 3.2.1, the spin state vector precesses around the z-axis with $\Delta\omega$. For the rest of this section, we assume $\Delta\omega \ll \Omega$.

We can use this behavior to measure the detuning $\Delta\omega$ between our excitation field and our spin level splitting with a so called *Ramsey sequence* (Figure 4 top): The spin is first initialized into its ground state, then rotated by a $\pi/2$-pulse onto the y-axis. During a pulse-free evolution time τ, the spin precesses in the x-y-plane by an angle

$$\phi = \tau \cdot \Delta\omega. \tag{14}$$

A last $\pi/2$-pulse is applied before the z-component is read out. During every subsequent iteration of the sequence, the waiting time τ is increased.

Starting at $\tau = 0$, we basically apply a π-pulse and therefore get $z = -1$. Increasing τ allows the spin to evolve after the first $\pi/2$-pulse so that the second $\pi/2$-rotation around the x-axis does

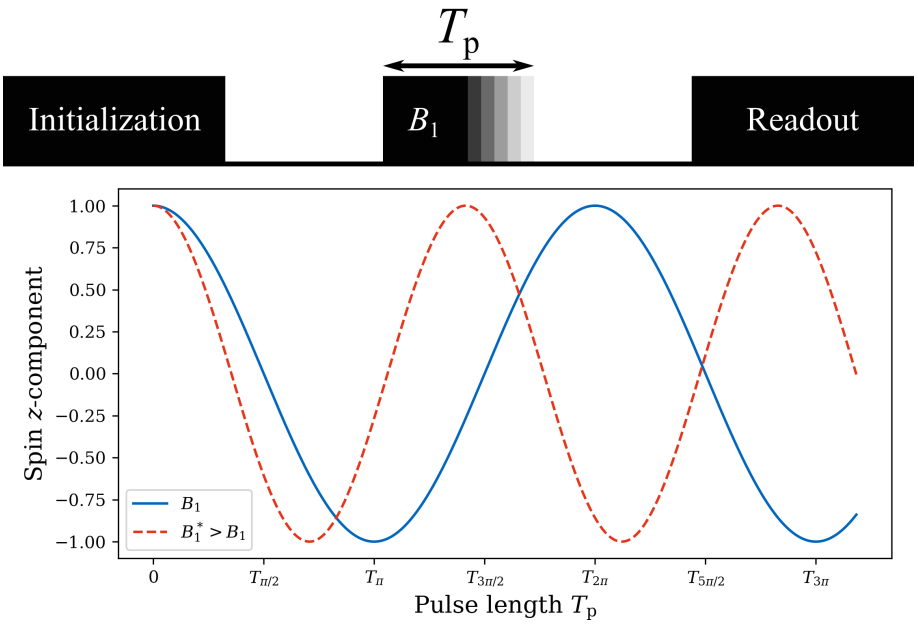

Figure 3: Rabi experiment. Top: Rabi sequence. It consists of initialization, an iteratively increasing driving field pulse and readout. Bottom: Measurement graph. The spin's rotation angle is linearly increased with pulse length, leading to a sinusoidal oscillation of its z-component. The abscissa ticks correspond to the blue graph recorded with field B_1. The oscillation frequency scales with the driving field, as indicated by the dashed red graph.

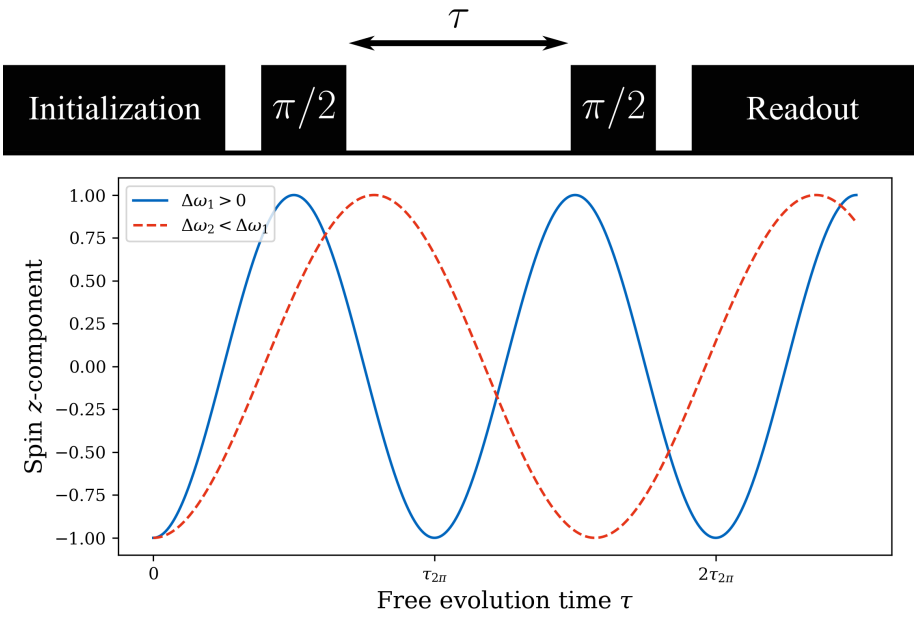

Figure 4: Ramsey experiment. Top: Ramsey sequence. It consists of initialization, two $\pi/2$-pulses with a free evolution time τ in-between and finally readout. Bottom: Measurement graph. During τ, the spin state is precessing with the detuning frequency $\Delta\omega$ and then projected onto the z-axis. As a result, the spin z-component is oscillating with the detuning frequency. The abscissa ticks correspond to the blue graph.

not fully excite the spin anymore. When τ is long enough for the spin to precess by an angle of $\phi = \pi/2$, the second $\pi/2$-pulse has no effect and we get a symmetrical superposition, i.e. $z = 0$. Further increasing τ decreases the excited state component until we get $z = 1$ for $\phi = \pi$. Increasing τ even beyond this level leads to an increase of the excited component again up until the spin is fully excited after a sequence for $\phi = 2\pi$.

The resulting measurement graph is an oscillation of the z-component again (Figure 4 bottom). In contrast to the previous section, the oscillation period is a measure for the detuning $\Delta\omega$, as described by equation 14. The oscillation period $\tau_{2\pi}$ directly translates into the detuning via

$$\Delta\omega = \frac{2\pi}{\tau_{2\pi}}. \tag{15}$$

3.3.3 Hahn Echo Sequence

As we will work with an inhomogeneous external magnetic field $\boldsymbol{B_0}(x, y, z)$ and a spatially distributed ensemble of spins, the resonance condition (equation 3) does also vary spatially. The resulting inhomogeneous detuning effects can however be compensated by a refocusing sequence such as the Hahn Echo sequence (Figure 5 top).

The spins are first initialized into their ground state, then rotated by a $\pi/2$-pulse onto the y-axis. Each spin of the ensemble starts precessing around the z-axis according to its local detuning

$$\Delta\omega(x, y, z) = \omega_{ph} - g_e \mu_B B_0(x, y, z) \tag{16}$$

during a first pulse-free waiting time τ_1, resulting in a distribution of phase angles ϕ (equation 14). A following π-pulse effectively inverts the y-component of each spin. During the following pulse-free waiting time τ_2, the inverted spins refocus due to the same individual local detuning $\Delta\omega(x, y, z)$ until they all overlap again at $\tau_1 = \tau_2$. A last $\pi/2$-pulse rotates the spins back onto the z-axis for readout. In the case of a constant vector field $B_0(x, y, z)$, the sequence with $\tau_1 = \tau_2$ rotates all spin vectors by 2π and they collectively end up in the ground state at $z = 1$ (Figure 5, upper graph).

This sequence is typically used to measure the spin-spin relaxation time T_2. If we fix $\tau_1 = \tau_2 = \tau$, we will find a decrease of the z-component of the states with increasing τ (Figure 5, lower graph). The main contributors to this decoherence effect are neighboring spins emitting nanoscale magnetic fields, whose quickly fluctuating influence can not be refocused by the sequence. The timescale of this exponential decrease is the so called spin-spin relaxation time T_2.

3.4 The Nitrogen-Vacancy Center

All the effects described above will be measured on the same physical system during this course: the nitrogen-vacancy (NV) center in diamond. It is a lattice defect, replacing two nearest-neighbor carbon atoms by a substitutional nitrogen atom and a vacancy. It is aligned along one of the ¡111¿-axis of the diamond. The NV electrons form an effective Spin 1 system. The corresponding energy level scheme consists of a ground state triplet $|g\rangle$, an excited state triplet $|e\rangle$ and a long lived shelving state $|s\rangle$ (Figure 6).

The $m_S = 0$ state of each triplet is already split from the $m_S = \pm 1$ states in the absence of any external magnetic field by the zero field splitting $D_{|g\rangle} = 2.87\,\text{GHz}$ and $D_{|e\rangle} = 1.42\,\text{GHz}$, respectively. The degeneracy of the $m_S = \pm 1$ states is lifted by applying a magnetic field $\boldsymbol{B_0}$ (Figure 6, green box). A state transition between the ground state's triplet's $m_S = 0$ state and one of its $m_S = \pm 1$ states is driven by resonant microwave radiation with frequency

$$\omega_{\text{mw}} = D_{|g\rangle} \pm \gamma_{\text{nv}} B_0, \tag{17}$$

where $\gamma_{\text{nv}} = 2.8\,\text{MHz/G}$ is the gyromagnetic ratio of the NV center. A spin conserving transition from $|g\rangle$ to $|e\rangle$ can be driven by light with a maximum wavelength of 638 nm. The excited $m_S = 0$ state almost exclusively radiatively decays back into its ground state pendant, providing one photon in the red spectrum. While the excited $m_S = \pm 1$ states share this decay channel, they also have a significant non-radiative decay channel via the shelving state, in which the spin remains for 300 ns before further non-radiatively decaying in the ground state, preferably the $m_S = 0$ state.

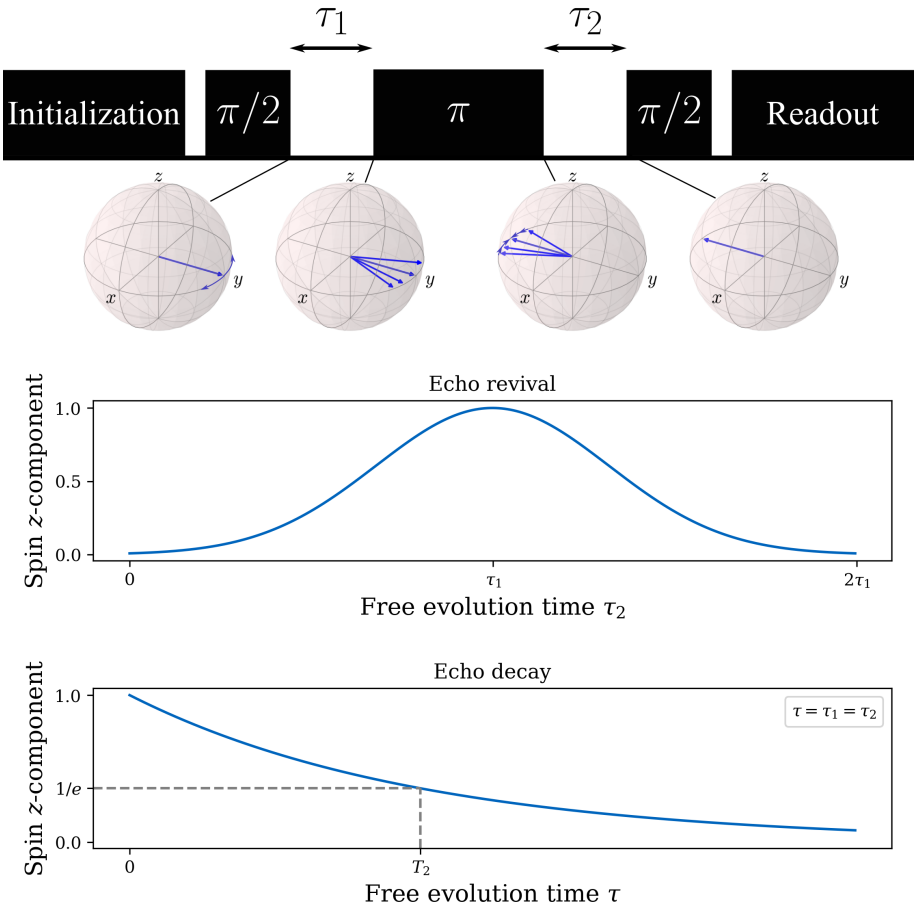

Figure 5: Hahn experiment. Top: Hahn echo sequence. The spheres below depict the spin states for given points of the sequence as blue arrows. After initialization, a $\pi/2$-pulse is applied and the spins are evolving during a first free evolution time τ_1 along the x-y-plane according to their local magnetic field $B_0(x, y, z)$. After a π-pulse they are evolving again during a second free evolution time τ_2, in general reverting the first evolution. After a second $\pi/2$-pulse, the collective spin state is read out. Upper graph: Echo revival measurement. The spin ensemble is best refocused if both evolution times are equal. This can experimentally be shown by fixing the value of τ_1 and sweeping τ_2 around this value. Lower graph: Echo decay measurement. The spin-spin relaxation time T_2 can be measured by fixing $\tau_1 = \tau_2$ and sweeping the evolution duration.

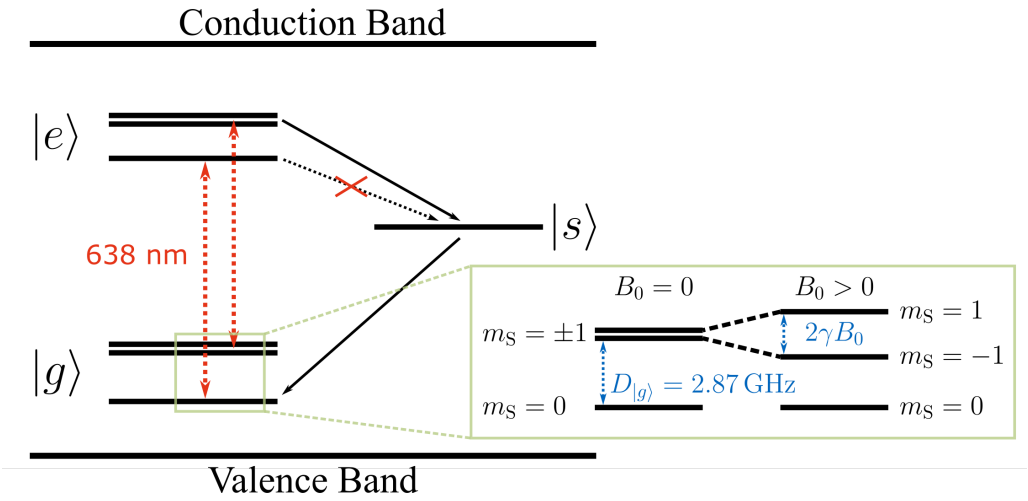

Figure 6: Level scheme of a NV center. Main plot: General level scheme. The band gap contains a ground state triplet $|g\rangle$, an excited state triplet $|e\rangle$ and a long-lived shelving state $|s\rangle$. Spin-conserving transitions between $|g\rangle$ and $|e\rangle$ can be optically driven. The $m_S = \pm 1$ states of $|e\rangle$ can additionally decay non-radiatively via $|s\rangle$ to the $m_S = 0$ state of $|g\rangle$. Green box: Zoom into the $|g\rangle$ state. At no external magnetic field, the $m_S = 0$ state is split by $D_{|g\rangle}$ from the degenerate $m_S = \pm 1$ states. The degeneracy is lifted by a field $B_0 > 0$.

These dynamics have two major applications: spin initialization and state readout. Spin initialization is achieved by continuously driving the optical transition. While the $m_S = 0$ is cycling unaltered between $|g\rangle$ and $|e\rangle$, the $m_S = \pm 1$ states will eventually decay into the shelving state and end up in the $m_S = 0$ state. Regardless of the original state, we can hence effectively initialize our spin into the $m_S = 0$ state.

Spin readout is achieved by collecting the photons emitted from the NV center during optical driving. As explained above, one $|g\rangle \rightarrow |e\rangle \rightarrow |g\rangle$ cycle provides one red photon emitted from the NV center. Thus, a spin in the $m_S = 0$ state provides one photon per cycle. A spin in a $m_S = \pm 1$ state will sometimes decay non-radiatively and therefore on average provide less than one photon per cycle. In summary, the NV center is brighter when it is in the $m_S = 0$ state than when it is in on of the $m_S = \pm 1$ states.

4 Experimental Setup

This section explains the fundamental functionality of the experimental setup of this lab course (Figure 7). The heart of the setup is a diamond sample with a considerable bulk NV center concentration. The optical transition of the NV centers is driven by a green laser ($\lambda = 520\,\mathrm{nm}$) focused on the diamond. The red photoluminescence emitted by the NV centers, carrying the spin state information, is recorded by a camera. A 650 nm long pass filter (not depicted) blocks the green excitation light. The microwave to manipulate the spin state inbetween a triplet comes from a continuous wave (cw) microwave generator and is chopped into pulses by a switch before it is applied to the NV centers via a ring antenna.

The whole setup is managed by a computer. It switches the laser on and off in cw mode or specifies the laser pulse sequence in pulsed mode. The computer also tunes the microwave source to the desired frequency and dictates the microwave pulse sequence generated by the switch. At last, the camera sends each recorded image to the computer where it is further processed and plotted as a graph as discussed in the theory section.

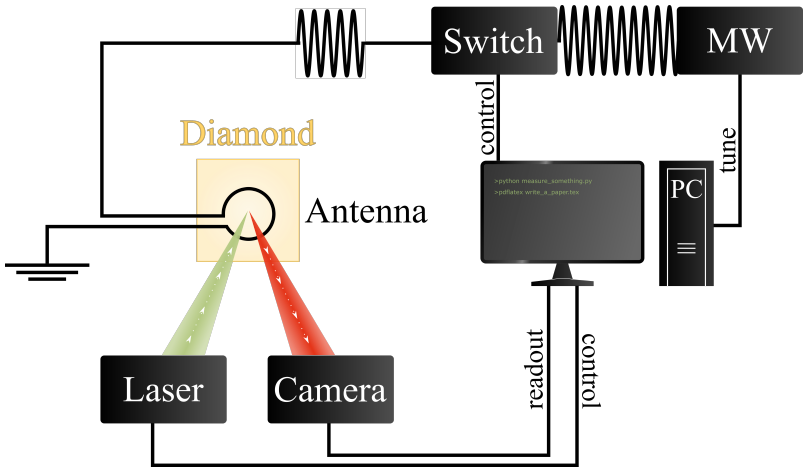

Figure 7: Experimental Setup. The NV centers in the diamond are optically excited by a laser, their spin is manipulated by a microwave pulses applied via an antenna and finally readout by a camera. The whole setup is managed by a computer.

5 Experimental Protocol

This section defines the experimental protocol for the laboratory time of this lab course. The first part treats the preparations to be met to ensure the technical apparatus is in good condition to perform the following measurements. The second part names the properties that need to be measured, however without going into detail. The actual procedure is to developed by the students in a discussion with the tutor during the lab course. Therefore it is vital to have read and understood sections 3 and 4.

5.1 Preparation

At first start the software by executing the corresponding 'main.py' file. Click on the 'Autoconnect' button, to connect the laser, the camera, the microwave source and the microwave switch.

5.1.1 Laser

Switch the laser on by clicking on the 'FPGA' button in the main window and then click on the 'On' button of the sub-window. Check if the laser spot is focused on the diamond and is surrounded by the ring antenna. If not, you can either move the diamond or the laser diode to correct their relative position. After moving, make sure, the antenna is pressed against the diamond.

5.1.2 Camera

Click on the 'Image' button of the main window. A sub-window with three panels appears. The left panel shows the live stream of the camera image, the middle panel shows the currently recorded background image and the right panel is the difference between the first two.

First, position the camera in such a way, that you see a sharp image of the laser spot. Use the sliders around the first panel to define your region of interest, which should be as narrow as possible around the laser spot. Now switch off the laser and record a background image.

If the image should show an intensity level of 64.000 counts, the camera is saturated in that spot. In this case you have to lower the exposure time in the camera settings.

5.1.3 Microwave

The microwave generation is performed by a voltage controlled oscillator (VCO). The output frequency is defined by a voltage applied at the VCO input. As a consequence, the software needs a voltage-frequency calibration. Click on the 'Microwave' button of the main window. The popped

up sub-window allows to load a recent calibration. If, during the measurement, the VCO calibration appears to be flawed, this window can also be used to recalibrate.

5.2 Measurement Tasks

1) Measure the zero field splitting $D_{|g\rangle}$.

2) Measure the effect of Zeeman splitting. Try to resolve the maximum number of resonance lines.

3) Determine the duration of a π-pulse.

4) Measure the detuning of your microwave frequency to one of the resonance lines.

5) Record an echo revival.

6 Additional Questions

Discuss the following questions in the protocol about this advanced lab course:

- Why is it impossible to measure the zero field splitting of the excited triplet state $D_{|e\rangle}$ with our setup?
- Discuss possible reasons, why the recorded Rabi oscillation does not continue endlessly?
- Can you imagine, how a Hahn echo can be used to detect a certain frequency instead of decoupling the system from it? (Hint: 'No' is not the correct answer.)